The four-component two-particle propagator for the calculation of double-ionization spectra of heavy-element compounds: I. Method

Markus Pernpointner

The four-component two-particle propagator for the calculation of double ionization spectra of heavy-element compounds I. Method.

Markus Pernpointner*

Theoretische Chemie, Universität Heidelberg,

Im Neuenheimer Feld 229, D-69120 Heidelberg, Germany

(Dated: August 23, 2010)

Abstract

In this work we present a new four-component implementation of the two-particle (2p) propagator as a powerful tool for calculating double ionization spectra of systems containing heavy elements. The 2p-propagator approach provides immediate access to the complete final state distribution of doubly ionized systems together with a detailed configurational information of each final state. This information is vital for the analysis of electronic decay processes as radiationless relaxation mechanisms after an initial core hole ionization and for the simulation of Auger spectra. The capabilities of the four-component realization is first demonstrated at the xenon atom and the bromine molecule for which experimental results are available. It turns out that a relativistic treatment is required for an adequate description of the experimental findings. In this first paper we focus on the electronic structure described by the 2p-propagator and will later on apply this method to the calculation of Auger spectra and electronic decay processes in heavy systems.

*Email:Markus.Pernpointner@pci.uni-heidelberg.de

I. INTRODUCTION

In the last few years modern experimental techniques such as double charge transfer spectroscopy [1–3], time-of-flight mass spectrometry [4], photoion and photoelectron coincidence spectroscopy [5–7] and threshold photoelectron coincidence (TPEsCO) [8] allowed for a detailed analysis of double ionization processes and a characterization of the resulting fragments. In these processes atoms, molecules or clusters are irradiated by photons of sufficient energy to produce at least two photoelectrons and dications that undergo fragmentation in most cases. The analysis of the photoelectrons and fragments yields a detailed insight into the ionization processes from an experimental viewpoint and is of prominent interest for the understanding of atmospheric chemistry, for example, where highly energetic radiation is initiating a multitude of chemical reactions. Of similar importance is the understanding of radiation damage in biological tissue also initiated by highly energetic primary ionization processes. In the case of CF_4, for example, the double ionization threshold was determined as 37.5 eV [8] and by photoion coincidence measurements the corresponding fragmentation products such as $CF_3^+ + F^+$ (37.6 eV) and $CF_2^+ + F^+$ (42.4 eV) could be identified. Simultaneous theoretical calculations with nonrelativistic Green's function techniques in combination with a two-hole ($2h$) population analysis [9] allowed for an accurate interpretation of the obtained experimental CF_4 spectrum. Other prominent examples for successful theoretical prediction and experimental analysis are the double ionization processes in formaldehyde [10], the interpretation of the spectrum in SF_6 [11], N_2O [12] and O_2 [13].

For all these systems the application of propagator methods turned out to be beneficial due to the accessibility of all dicationic states and their composition after a single matrix diagonalization. For the CF_4 molecule a final state analysis showed a prevailing hole localization on the fluorine atoms with only minor carbon contributions. Coincidence maps further allow for a classification in direct and indirect ionization processes depending on the photon energy as has been shown for SF_6 [11]. Here the indirect mechanism via a primary ionization of the F $2s$ level followed by an electronic decay could be established. These decay mechanisms are accurately predicted by the current theoretical methods and play a major role in the correct interpretation of the spectra.

Recently, experimentalists started to analyze double ionization spectra of heavier systems

such as molecular bromine [14, 15] and iodine [16], the interhalogen compound ICl [17] and the iodine-containing systems HI, CH_3I and CF_3I [18]. For the doubly ionized final states of ICl state-specific multi-reference configuration interaction (MRCI) methods were employed by Edvardsson et al. [17] where the $X^3\Sigma^-_{0,1}$, $A^1\Delta_2$ and $B^1\Sigma^+_0$ states could be clearly identified in the outermost part of the spectrum between 27 eV and 29 eV. Above 30 eV the assignments were done tentatively. The potential curves give precise information about the boundedness of a specific state but it is more difficult to decide about further electronic decay processes and the nature of states at higher energy ranges.

Another prominent example for double ionization processes in systems with heavy elements are the methyl iodide CH_3I and trifluoro methyl iodide CF_3I spectra which were measured by the TOF-PEPECO (time-of-flight photoelectron coincidence) method [18]. Whereas in the methyl iodide spectrum four well resolved peaks of symmetry $^3A_2$ (spin-orbit split in an A_1 and E state), ^1E and $^1A_1$ occur, the CF_3I^{2+} shows a more complicated structure with five peaks including spin-orbit splitting and a broad ionisation edge. The authors in [18] attribute the extra peaks to final states where one hole is each located on the iodine and fluorine atom leading to a dication with considerably lowered Coulomb repulsion compared to the purely iodine-centered dicationic state.

Doubly ionized clusters often result from an electronic decay process following a primary ionization on one site. Hereby the Intermolecular Coulombic Decay (ICD) [19] or the Electron Transfer Mediated Decay (ETMD) [20] are the most prominent examples of these decay processes currently investigated. These processes are normally initiated by a inner valence ionization where the vacancy is filled by an outer valence electron from the same site (ICD) or from a neighboring site (ETMD). The released energy is hereby sufficient to ionize the system further where in general many decay channels are open. It sould be kept in mind that the accessibility and characterization of the possible final states will also depend on the inclusion of relativistic effects.

In order to treat the abovementioned systems containing heavy elements adequately a four-component implementation of the two-particle propagator was undertaken and is presented in this work. Hereby access to the full spectrum together with a detailed configuration information of the final states is obtained. Relativity will have substantial influence on the energetics of the resulting final states which in turn determine the structure of the spectra and the accessibility of decay pathways. In the following we first outline the relativistic

methodology of the $2h$ propagator together with a focus on the symmetry handling in the double group-based framework. Afterwards, the double ionization spectra of xenon and Br_2 are calculated in order to demonstrate the capabilities of the method. For Br_2 double group configuration interaction (CI) and multi-reference coupled cluster (MRCC) calculations are also available [21] and allow for a comparison with our results. In subsequent work we will address relativistic effects in the double ionization spectra of CH_3I, CF_3I, I_2 and ICl and their impact on ICD/ETMD processes in clusters containing heavy elements.

II. METHODOLOGY IN THE RELATIVISTIC CASE

The two-particle propagator or Green's function describing a double ionization or attachment process reads as

$$G_{pq,p'q'}(t_1,t_2;t_1',t_2') = -\langle \Psi_0^N | \hat{T} \left[c_p(t_1) c_q(t_2) c_{q'}^\dagger(t_2') c_{p'}^\dagger(t_1') \right] | \Psi_0^N \rangle \,, \tag{1}$$

with $|\Psi_0^N\rangle$ being the *exact* N-particle ground state wave function of the Dirac-Coulomb (DC) operator

$$\hat{H}_{DC} = \sum_{i=1}^{N} \left(c\vec{\alpha}_i \cdot \vec{p}_i + \beta_i m_e c^2 + V_{\text{ext}}(i) \mathbf{1}_4 \right) + \sum_{i<j}^{N} \frac{1}{r_{ij}} \,, \tag{2}$$

where magnetic interaction (Gaunt) corrections to the Coulomb term and retardation effects are neglected. $\hat{T}$ is the Wick time-ordering operator and the $c_q^\dagger(t)$ $[c_q(t)]$ denote creation (destruction) operators for one-particle states $|\phi(q)\rangle$ in the Heisenberg representation. In the language of second quantization in which the algorithm is cast no excitations from negative energy states are considered (see [22] for the no-pair formalism in combination with propagators and [23] for an analysis of the general unboundedness problem in case of the DC operator).

For the practical implementation one starts form the energy-dependent representation of (1) obtained by a Fourier transformation:

$$\Pi_{pq,p'q'}(\omega) = \Pi^+_{pq,p'q'}(\omega) + \Pi^-_{pq,p'q'}(\omega) \,.$$

$\Pi^+_{pq,p'q'}(\omega)$ hereby describes a two-particle attachment whereas $\Pi^-_{pq,p'q'}(\omega)$ is used for a two-particle detachment (ionization) process. The Lehmann representation [24] of $\Pi^-_{pq,p'q'}(\omega)$

which we are focusing on in this work reads as

$$\Pi^{-}_{pq,p'q'}(\omega) = -\sum_{m} \frac{x^{(m)}_{pq} x^{(m)*}_{p'q'}}{\omega + E^{N-2}_{m} - E^{0}_{N} - i\eta} \tag{3}$$

utilizing a complete set of *exact* $N-2$ particle states $|\Psi^{N-2}_{m}\rangle$ with corresponding energies E^{N-2}_{m}. η is an infinitesimal positive number required for the convergence of the backtransformation. The spectral amplitudes

$$x^{(m)}_{pq} = \langle \Psi^{N-2}_{m} | c_p c_q | \Psi^{N}_{0} \rangle$$

provide information about the composition of the mth final state with respect to the one-particle states p and q. It should be pointed out that the N-particle ground state wave function $|\Psi^{N}_{0}\rangle$ can be expanded in a N-particle basis of Slater determinants made of four-component one-particle functions. The no-pair confinement puts us into the advantageous situation that the spin-orbital based expressions derived from diagrammatic perturbation theory need not be modified for a corresponding realization with four-component one-particle functions.

Up to this stage we have not yet obtained actual expressions for the propagator. This is established by a combination of the diagrammatic representation for Π^{-} together with an algebraically formulated perturbation expansion of a nondiagonal representation of (3) termed as Algebraic Diagrammatic Construction (ADC) [25–28]. In a compact matrix notation (3) reads as

$$\underline{\Pi}^{-}(\omega) = \underline{X}^{\dagger}(\omega\underline{1} + \underline{\Omega})^{-1}\underline{X}$$

with $\underline{1}$ being the identity matrix and $\underline{\Omega}$ being the diagonal matrix of double ionization potentials. This diagonal representation is now brought into a nondiagonal form by inserting a so-called intermediate state basis [29] leading to

$$\underline{\Pi}^{-}(\omega) = \underline{F}^{\dagger}(\omega\underline{1} - \underline{\Gamma})^{-1}\underline{F}\,.$$

A perturbational expansion of the $\underline{\Gamma}$ and $\underline{F}$ matrices then allows for an order-by-order comparison to the graphs obtained by a diagrammatic perturbation expansion from which the explicit expressions for the matrix elements can be derived [25, 30]. The $\underline{F}$ matrices are needed for the calculation of transition moments and are disregarded for the current investigation. A final matrix diagonalization then yields the sought double ionization potentials

together with the eigenvectors containing the expansion coefficients of the mth eigenstate in terms of the intermediate basis. A specific eigenstate in the intermediate state basis can also be expanded in a perturbation series starting with a two-hole Slater determinant in zeroth order and where the additional terms account for electron relaxation and correlation [31]. If a specific final state exhibits main state character, $3h1p$ configurations mix in only weakly whereas other $2h$ configurations may participate substantially as the calculations show. The Algebraic Diagrammatic Construction in its four-component extension will be termed as Dirac-Coulomb ADC (DC-ADC).

Similar to other post-Hartree-Fock methods like coupled cluster (CC) or configuration interaction (CI) an atomic orbital (AO) to molecular orbital (MO) transformation step is also required in DC-ADC yielding relativistic molecular two-electron integrals over the Coulomb operator

$$V_{abcd} = \iint \phi_a^*(1)\phi_b^*(2)\frac{1}{r_{12}}\phi_c(1)\phi_d(2) \equiv \langle ab|cd\rangle \tag{4}$$

and their totally antisymmetric versions used in the implementation

$$V_{ab[cd]} = V_{abcd} - V_{abdc} \equiv \langle ab||cd\rangle \,. \tag{5}$$

The $V_{ab[cd]}$ integrals exhibit the relations

$$V_{ab[cd]} = -V_{ab[dc]} = -V_{ba[cd]} = V_{ba[dc]} \quad \text{and} \quad V_{cd[ab]} = V^*_{ab[cd]} \,. \tag{6}$$

The indices a, b, c, d hereby cover the occupied and/or the virtual orbital space. The totally antisymmetric MO integrals together with the (relativistic) spinor energies ϵ_a are the only entities entering the expressions for the DC-ADC matrix elements which were originally derived in the nonrelativistic regime by Schirmer and Barth [25] and restated by Tarantelli [28] with an appropriate sign change in order to obtain positive eigenvalues of the ADC matrix. In [28] both the spin-containing and spin-free formulas can be found where in the latter case two different sets of equations for the singlet and triplet final states result. This classification according to spin multiplicity is no longer applicable for heavy systems with large spin-orbit coupling and the spin-orbital-based expressions are to be employed in the four-component case. It should be kept in mind that the AO/MO transformation is done exclusively in the positive energy space utilizing the corresponding Dirac-Hartree-Fock spinors. As a consequence, the molecular spinors can not be further relaxed with respect to the negative energy solutions in the ADC step which might yield to changes in

the ionization potentials for very heavy systems and core-like final states. In the valence region these additional contributions are assumed to be small and the electron relaxation and correlation effects are completely covered by the propagator. In the following we will often refer to the equations given in [28] and we will therefore repeat them here for convenience in eqs. (7) - (9). The three equations comprise the $2h/2h$ main block $C_{ij,kl}$ (7), the $3h1p/2h$ coupling block $C_{rklm,ij}$ (8) and the $3h1p/3h1p$ satellite block $C_{rijk,slmn}$ (9) of the DC-ADC matrix. In the following the indices $i, j, k, \ldots$ refer to occupied (hole) orbitals, the indices $p, q, r, \ldots$ to virtual (particle) orbitals and $\epsilon_{ijk\ldots}$ is an abbreviation for $\epsilon_i + \epsilon_j + \epsilon_k + \cdots$.

$$
\begin{aligned}
C_{ij,kl} &= V_{ij[kl]} + \left\{ \delta_{jl} \frac{1}{2} \sum_{mrs} \frac{V_{rs[km]} V_{im[rs]}}{(\epsilon_{rs} - \epsilon_{km})(\epsilon_{rs} - \epsilon_{im})} \left[\epsilon_{rs} - \epsilon_m - \frac{\epsilon_{ik}}{2} \right] \right\} \qquad (7) \\
&\quad - \{i \leftrightarrow j\} - \{k \leftrightarrow l\} + \{i \leftrightarrow j, k \leftrightarrow l\} \\
&\quad - \frac{1}{2} \sum_{rs} \frac{V_{rs[kl]} V_{ij[rs]}}{(\epsilon_{rs} - \epsilon_{kl})(\epsilon_{rs} - \epsilon_{ij})} \left[\epsilon_{rs} - \frac{\epsilon_{ijkl}}{2} \right] - \delta_{ik} \delta_{jl} \epsilon_{ij} \, . \\
C_{rklm,ij} &= \left(\delta_{ik} V_{lm[jr]} + \delta_{il} V_{mk[jr]} + \delta_{im} V_{kl[jr]} \right) - (i \leftrightarrow j) \, . \qquad (8) \\
C_{rijk,slmn} &= \left\{ \delta_{rs} \left[\delta_{il} V_{jk[mn]} + \delta_{im} V_{jk[nl]} + \delta_{in} V_{jk[lm]} \right] \right\} \qquad (9) \\
&\quad + \{(i,j,k) \to (j,k,i)\} + \{(i,j,k) \to (k,i,j)\} \\
&\quad + \left\{ \delta_{jm} \delta_{kn} V_{is[rl]} + \delta_{jl} \delta_{km} V_{is[rn]} - \delta_{jl} \delta_{kn} V_{is[rm]} \right\} \\
&\quad + \{(i,j,k) \to (k,i,j)\} - \{i \leftrightarrow j\} \\
&\quad + \delta_{rs} \delta_{il} \delta_{jm} \delta_{kn} (\epsilon_r - \epsilon_{ijk}) \, .
\end{aligned}
$$

The abbreviation $\{i \leftrightarrow j\}$ in (7) - (9) hereby symbolizes an i, j swapping of the preceding expression cast in curly brackets and $(i, j, k) \to (k, i, j)$ stands for the index replacements as indicated. For the numerical realization the 2- and 4-tuples $ij, \ldots$ and $rijk, \ldots$ are to be understood as multi-indices addressing rows and columns of the DC-ADC matrix in a unique way. The expressions (7) - (9) are complete up to second order in perturbation theory (DC-ADC2) and contain additional first order contributions in the satellite block not present in the strict second order formulation.

A fundamental property of all matrix elements above is their antisymmetry with respect to hole-index interchange within the bra or ket space (not between these spaces, of course). In equation (8), for example, we end up with the identities $C_{rklm,ij} = -C_{rlkm,ij} = -C_{rklm,ji} = \ldots$. As a consequence, matrix elements vanish identically if two or more of their hole indices are equal. It is important for the implementation to omit all permutationally related or zero

terms in the DC-ADC matrix which can be achieved by following a restricted enumeration scheme for the multi-indices. For example, in the $(rklm)$ multi-index the confinements $k > l > m \,\forall\, r \in \{virt\} \wedge k, l, m \in \{occ\}$ have to be obeyed.

One major factor essentially governing our realization is molecular symmetry which is fully exploited up to all Abelian subgroups of the D_{2h}^* double group. Since the molecular spinors transform according to the molecular double group $\mathcal{G}^*$ and not according to the single-valued counterpart $\mathcal{G}$ the use of double groups containing so-called extra or fermionic irreducible representations (irreps) γ_i is mandatory for DC-ADC. The single-valued counterpart $\mathcal{G}$ of $\mathcal{G}^*$ contains the bosonic irreps $\beta_i \in \mathcal{G}$. All irreps of Abelian subgroups to $\mathcal{G}^*$ are one-dimensional and exhibit the following useful property:

$$\gamma_i^* \otimes \gamma_i = \Gamma_0\,, \gamma_i \in \mathcal{G}^* \qquad \text{and} \qquad \beta_i^* \otimes \beta_i = \Gamma_0\,, \beta_i \in \mathcal{G} \tag{10}$$

with Γ_0 being the totally symmetric irrep of $\mathcal{G}^*(\mathcal{G})$. The complex conjugate of an irrep therefore is its own inverse allowing for a fast computation of target irreps being part of a multiple direct product. Furthermore, the direct product of two fermionic (bosonic) irreps yields a bosonic irrep, whereas the mixed product yields a fermionic irrep. The highest available point group symmetry in the employed DIRAC program package [32] is D_{2h}^* followed by D_2^* and C_{2v}^*. The bosonic irreps of these groups are one-dimensional and the corresponding bosonic subgroups therefore are Abelian. However, for the corresponding fermionic representations nonseparable two-dimensional irreps are obtained not leading to an overall Abelian group structure anymore. This can be seen, for example, in the C_{2v}^* group where $E_{1/2} \otimes E_{1/2}$ yields a four-dimensional reducible representation which can be decomposed into $A_1 \oplus A_2 \oplus B_1 \oplus B_2$. Therefore a projection of the non-Abelian double groups to their Abelian subgroups is performed according to $D_{2h}^* \rightarrow C_{2h}^*$, $D_2^* \rightarrow C_2^*$ and $C_{2v}^* \rightarrow C_2^*$. For these subgroups the number of fermionic and bosonic irreps is identical and their sum equals the number of classes in $\mathcal{G}^*$ allowing for an efficient symmetry handling.

In our implementation the storage of integrals and the tensorial contractions are symmetry-driven. In order to demonstrate this for the $V_{ij[kl]}$ integrals as a representative example one always follows the all-encompassing requirement

$$\gamma_i^* \otimes \gamma_j^* \otimes \gamma_k \otimes \gamma_l \stackrel{!}{=} \Gamma_0\,, \tag{11}$$

otherwise $V_{ij[kl]}$ vanishes. For defining a label-free storage sequence we simply follow the generic order $(\gamma_1, \ldots, \gamma_N)$ starting with the rightmost irrep $\gamma_l \in \mathcal{G}^*$. The subsequent irreps

γ_k, γ_j^* and γ_i^* are then looped over accordingly always maintaining relation (11) where the irreps γ_i and γ_j have to be taken as complex conjugates due to their relation to the bra space. For a two-indexed array $\langle i|j\rangle$ we then obtain the following storage scheme with respect to the irrep sequence:

$$\langle i|j\rangle : \gamma_1^*|\gamma_1,\, \gamma_2^*|\gamma_2,\, \ldots, \gamma_N^*|\gamma_N \quad \text{with} \quad \gamma_q^* \otimes \gamma_q = \Gamma_0\,.$$

In the case of four-index quantities $\langle ij||kl\rangle$ the situation is a bit more complex since on the bra and on the ket side the two fermionic irreps first combine to bosonic irreps which in turn are again stored in generic order:

$$\langle ij||kl\rangle : \beta_1^{(ij)*}|\beta_1^{(kl)}, \beta_2^{(ij)*}|\beta_2^{(kl)}, \ldots \beta_N^{(ij)*}|\beta_N^{(kl)} \quad \text{with} \quad \beta_q^{(ij)*} \otimes \beta_q^{(kl)} = \Gamma_0\,.$$

Hereby the superscripts (ij) and (kl) indicate the fermionic parent irreps and the subscripts enumerate the bosonic irreps. For a given β_q we recursively apply this logic again and obtain a stream sequence like

$$\beta_q^{(ij)} : \gamma_{i_1}|\gamma_1, \gamma_{i_2}|\gamma_2, \ldots \gamma_{i_N}|\gamma_N \quad \text{with} \quad \gamma_{i_k} \otimes \gamma_j \stackrel{!}{=} \beta_q^{(ij)}\,. \tag{12}$$

Both fermionic irreps producing $\beta_q^{(ij)}$ either stem from the bra or from the ket space and relation (12) also applies to the bra space after complex conjugation. As soon as the smallest symmetry cell, $\gamma_{i_k}|\gamma_j$, is established the individual spinors occurring therein are enumerated generically completing the index-free storage scheme. This label-free storage is also applied for the relativistic coupled cluster [33] and configuration interaction module in the DIRAC program suite [32].

In the general two-electron integral $V_{ab[cd]}$ the indices a, b, c, d stand for occupied (O) or virtual (V) orbitals. It is evident from Eqs. (7)-(9) that only four distinct integral classes, namely the $\langle OO||OO\rangle, \langle VO||OO\rangle, \langle VV||OO\rangle$ and $\langle VO||VO\rangle$ types are needed for the construction of the matrix elements. Hereby the $\langle VV||OO\rangle$ and $\langle VO||VO\rangle$ classes are essentially distinct due to the different bra and ket origin of the O and V spinors. Every other order of indices such as e.g. $V_{is[rm]}$ with $i, m \in \{occ\}$, $r, s \in \{virt\}$ can be brought into one of the four generic forms utilizing the equivalence relations (6). The matrix elements of Eqs. (7)-(9) are therefore transformed to a form suitable for direct use of the four generic integral classes.

One very important property of the total ADC matrix which holds in the one- and four-component case is its block structure with respect to different bosonic final state symmetries

(see Fig. 1). Hereby no coupling between blocks of different symmetry occurs which can be seen as a consequence of relation (11). By this grouping into disjoint blocks the numerical effort for the matrix diagonalization is drastically reduced. It should be noted that the symbols $I_2, J_2, \ldots$ in Fig. 1 stand for the twofold and fourfold multi-indices of Eqs. (7)-(9) in exactly the same index ordering. The symmetry requirements for nonvanishing $2h/2h$ matrix elements $C_{ij,kl}$ of Eq. (7) now read as

$$\text{bra} : \beta_1^{(ij)*} = \gamma_i^* \otimes \gamma_j^* \,, \quad \text{ket} : \beta_2^{(kl)} = \gamma_k \otimes \gamma_l \,, \quad \beta_1^{(ij)*} \otimes \beta_2^{(kl)} \stackrel{!}{=} \Gamma_0 \,. \tag{13}$$

After multiplying the last equation by $\beta_1^{(ij)}$ and considering (10) we obtain relations for the bra and ket irreps in order to obtain nonvanishing matrix elements as

$$\beta_1 := \beta_1^{(ij)} \stackrel{!}{=} \beta_2^{(kl)} =: \beta_2 \,.$$

This holds for all available bosonic irreps β_q in $\mathcal{G}^*, q = 1, \ldots N$ leading to the block structure. The present considerations can be applied in a similar way to the coupling and satellite blocks where care must be taken to perform integral contractions exclusively over corresponding bra/ket pairs. The transition from Abrikosov diagrams to their algebraic counterpart exactly determines the position of a specific spinor index in the bra or ket space. The left-hand-side occurrence of the $(rklm)$ multi-index in $C_{rklm,ij}$ (Eq. 8), for example, does not automatically imply a bra character for them. Instead, from Eq. (8) the correct bra/ket sequence for this multi-index can be derived according to

$$C_{rklm,ij} : \quad (rklm, ij) \leftrightarrow |\rangle\langle|\langle|\langle|, |\rangle|\rangle \tag{14}$$

and the symmetry conditions are established as

$$\gamma_r \otimes \gamma_k^* \otimes \gamma_l^* \otimes \gamma_m^* \otimes \gamma_i \otimes \gamma_j \stackrel{!}{=} \Gamma_0 \,. \tag{15}$$

The pair γ_i, γ_j hereby defines the final state symmetry $\beta_f := \beta_q^{(ij)} = \gamma_i \otimes \gamma_j$ of the DC-ADC matrix block. In order not to omit contributions we loop through all possible $(\gamma_k, \gamma_l, \gamma_m)$ triples and fix γ_r after complex conjugation of (15) via

$$\gamma_r^* \otimes \gamma_{klm} = \beta_f \quad \text{with} \quad \gamma_{klm} = \gamma_k \otimes \gamma_l \otimes \gamma_m \quad \Longrightarrow \quad \gamma_r = \beta_f^* \otimes \gamma_{klm} \,.$$

The numerous delta-conditions in the satellite block (9) test for like spinor labels which are a priori not available in a purely symmetry-driven storage. Since the DC-ADC matrix is

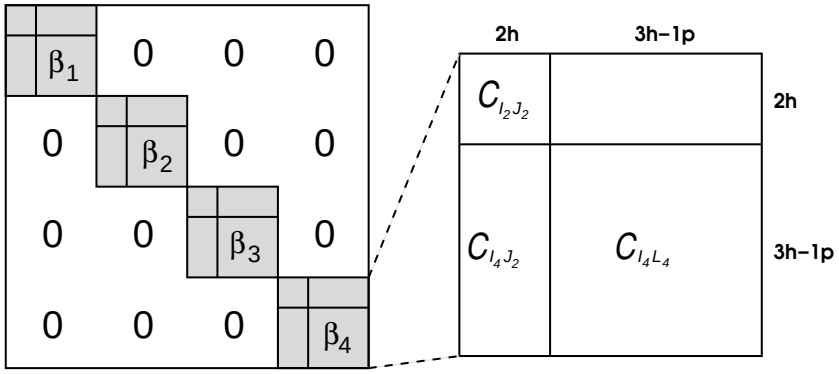

FIG. 1: Illustration of the symmetry block formation of the total ADC matrix with respect to the final state irreps β_i. The symbols I_2, J_2 (I_4, L_4) denote the twofold (fourfold) multi-indices from Eqs. (7)-(9).

to be constructed for each Lanczos iteration and to be stored in a packed row/column form on disk it is more efficient to utilize a row/column-based addressing in the satellite block and recover the spinor index quadruple via a lookup table whenever needed.

III. COMPUTATIONAL DETAILS

For all calculations the Dirac-Coulomb Hamiltonian with inclusion of the $(SS|SS)$ integrals was employed and the relevance of spin-orbit effects was demonstrated by additionally performing ADC2 calculations with an underlying spin-free Hamiltonian by Dyall [34, 35]. In the latter case only scalar relativistic effects are taken into account and the symmetry is governed by the normal group instead of the double group. For xenon the dual-type $(26s21p16d4f4g2h)$ primitive exponent set from [36] was used and is shown in table I. The duality condition hereby restricts the exponent sets according to $\{d\} \subset \{s\}, \{f\} \subset \{p\}, \{g\} \subset \{s\}$ and $\{h\} \subset \{p\}$ by which the number of $(SS|SS)$ integrals to be determined in a four-component calculation can be considerably reduced. Spinors in the energy range from -10.0 a.u. up to +100.0 a.u. were taken into account for the electron correlation treatment which corresponds to an inclusion of all occupied Xe orbitals with $n \geq 4$.

For the bromine molecule the Dyall $(23s16p10d1f)$ triple zeta basis set [37] was taken in its uncontracted form and all spinors in the energy range of -4.0 a.u. to +10.0 a.u. were included in the active correlation space. It should be kept in mind that a molecular

s exponents	58489121.56, 12439351.36, 3316966.28, 990057.5054, 324445.4957, 114591.3996, 43146.79011, 17136.16529, 7100.746012, 3039.568325, 1338.816396, 606.7452457, 281.9892934, 134.2794051, 65.33858323, 32.35300441, 16.27465179, 8.322702468, 4.136039210, 1.996937059, 0.9255024105, 0.3746212971, 0.1430107603, 0.0656456, 0.0326239, 0.0112533
p exponents	1463134.8, 213759.6455, 45317.14034, 12192.17836, 3947.39928, 1469.89679, 606.2137536, 269.3317758, 125.9350996, 60.95699859, 29.54636251, 14.616124, 7.355676352, 3.483210105, 1.624885916, 0.6565235892, 0.2871010293, 0.1115846738, 0.04188980896, 0.025, 0.011
d exponents: $\{s10 - s25\}$	f exponents: $\{p15 - p18\}$
g exponents: $\{s21 - s24\}$	h exponents: $\{p16 - p17\}$

TABLE I: Dual primitive exponent set for xenon used in the DC-ADC2 calculations. The notation $\{s10 - s25\}$ hereby indicates the s exponent range used for the d functions asf.

calculation is much more elaborate than an atomic one and the range of active spinors therefore had to be restricted accordingly. The experimental distance of $R = 2.28105$Å [38] was taken for the Br_2 calculations.

All electronic structure calculations have been carried out with the program system DIRAC [32] which is a general-purpose four-component package. The relativistic implementation of the two-particle propagator DC-ADC2 is available in the developers' version at the moment and will soon be part of the official release. In addition to spatial symmetry time-reversal symmetry is exploited throughout the DC-ADC2 code. In the current implementation DIRAC also supports linear symmetry which allows for a Ω-coupled final state classification of the bromine molecule and also for a M_J classification in the xenon atom.

IV. RESULTS AND DISCUSSION

A. Xenon

As a first application we provide theoretical DC-ADC2 results for the Xe^{2+} final states and corresponding line spacings together with a simulated double ionization spectrum of Xe in the low energy regime comprising the $5p^4$ configuration. Experimental levels and transitions were obtained by Persson et al. [39] who also performed theoretical calculations based on Hartree-Fock theory with inclusion of some configuration interaction effects. These energy levels also served for the determination of a xenon $N_{4,5}OO$ Auger spectrum [40]. In table II we collect the experimental data by Persson et al. for the *gerade* final states and our theoretical results obtained by the DC-ADC2 procedure. Uncorrelated self-consistent field results (DC-SCF) are also given and stress the relevance of electron correlation contributions. All states listed emerge from a valence doubly ionized $5s^25p^4$ configuration (nonrelativistic notation) leading to possible $(5p_{\frac{1}{2}})^2(5p_{\frac{3}{2}})^2$, $(5p_{\frac{1}{2}})^1(5p_{\frac{3}{2}})^3$ and $(5p_{\frac{1}{2}})^0(5p_{\frac{3}{2}})^4$ occupations in the jj-coupled case.

J level	Exp. [39]	DC-SCF	DC-ADC2	Δ(DC-SCF)	Δ(DC-ADC2)
$^3P_0$	8130.08	8929.7	8493.01	799.64	362.93
$^3P_1$	9794.36	9657.7	9627.03	-136.64	-167.33
$^1D_2$	17098.73	19689.1	17344.14	2590.4	245.41
$^1S_0$	36102.94	41052.3	37840.29	4949.3	1737.35

TABLE II: Experimental and theoretical transition energies (in cm^{-1}) from the lowest $(5p_{\frac{1}{2}})^2(5p_{\frac{3}{2}})^2\ ^3P_2$ reference state to the various excited states with $J = 0, 1, 2, 0$. Uncorrelated (DC-SCF) and correlated (DC-ADC2) results are included. In the last two columns the difference to the experimental value is shown stressing the relevance of electron correlation contributions.

The inadequacy of a pure LS coupling scheme can be seen in table II where the individual J terms belonging to a specific ^{2S+1}L manifold are significantly separated (the splitting of the $5p_{1/2}$ and $5p_{3/2}$ spinors in neutral xenon amounts to 1.44 eV at the DC-SCF level). We note that the obtained energetic order in a relativistic description is identical to the experimental one (see table II) and the corresponding level spacings at the correlated DC-ADC2 level are in much better agreement to experiment than they are for an uncorrelated description

(DC-SCF).

J level	Energy cm^{-1}	CSF
2	0.0	0.95185 Φ_2 + 0.30657 Φ_3
0	8929.7	0.84705 Φ_1 - 0.53151 Φ_5
1	9657.7	1.00000 Φ_4
2	19689.1	-0.30657 Φ_2 + 0.95185 Φ_3
0	41052.3	0.53151 Φ_1 + 0.84705 Φ_5

TABLE III: Composition of the J-adapted CSFs at the DC-SCF level. $\Phi_1 = p^2_{\frac{1}{2}} p^2_{\frac{3}{2}} (J = 0)$, $\Phi_2 = p^2_{\frac{1}{2}} p^2_{\frac{3}{2}} (J = 2)$, $\Phi_3 = p^1_{\frac{1}{2}} p^3_{\frac{3}{2}} (J = 2)$, $\Phi_4 = p^1_{\frac{1}{2}} p^3_{\frac{3}{2}} (J = 1)$, $\Phi_5 = p^0_{\frac{1}{2}} p^4_{\frac{3}{2}} (J = 0)$

Adapting the jj coupling scheme we expect configurations belonging to the same J value to mix as observed at the Dirac-Hartree-Fock level already. In a relativistic average open shell calculation of the xenon [core]$(5p)^4$ electron configuration (e.g. with GRASP [41, 42]) the CSFs for individual J levels are mixtures of different two-particle jj-coupled Slater determinants (see table III for the atomic results). This multi-configurational character will also transfer to the propagator results.

In table IV a relativistic final state analysis for the $5p^4$ configuration is presented where the spinors carrying the holes are listed. The calculated final states all possess main state character and genuine $2h$ configurations are strongly prevailing over $3h1p$ admixtures. Since the calculations were performed applying linear symmetry we have immediate access to the projection of the total angular momentum J onto the z axis. These different M_J values occur in separate irreps allowing for a detailed classification of the final states. For example, a DC-SCF calculation of the $J = 2$ ground state yields a $0.95 p^2_{1/2} p^2_{3/2} + 0.31 p^1_{1/2} p^3_{3/2}$ state composition. According to the notation in table IV this corresponds to a $p(m_{j_1})p(m_{j_2})$ and a $p(m_{j_1})\bar{p}(m_{j_2})$ $2h$ state. As in the DC-SCF case the $p(m_{j_1})p(m_{j_2})$ configuration remains the dominant part of the Xe^{2+} ground state for all M_J projections (in the case of $M_J = 0$ there are two realizations with respect to the individual m_j projections but the sum of the squares is identical to the square of the $M_J \neq 0$ contributions) and therefore shows resemblance to the DC-SCF ground state with respect to the configuration mixing. However, the decrease of the pole strength from unity to 0.8818 clearly indicates contributions from other $2h$ and $3h1p$ states accounting for electron correlation. Due to their large number and smallness

they are not listed in table IV.

DIP	PS	Configurations	M_J
32.7964	0.8818	-0.1786 $p(-\frac{1}{2})\bar{p}(\frac{1}{2})$ -0.1786 $\bar{p}(-\frac{1}{2})p(\frac{1}{2})$ -0.6395 $p(-\frac{1}{2})p(\frac{1}{2})$ -0.6395 $p(-\frac{3}{2})p(\frac{3}{2})$	0
32.7964	0.8818	0.2187 $p(\frac{1}{2})\bar{p}(\frac{1}{2})$ +0.1263 $p(\frac{3}{2})\bar{p}(-\frac{1}{2})$ +0.9044 $p(\frac{3}{2})p(-\frac{1}{2})$	+1
32.7964	0.8818	-0.1263 $p(-\frac{3}{2})\bar{p}(\frac{1}{2})$ -0.9044 $p(-\frac{3}{2})p(\frac{1}{2})$ -0.2187 $p(-\frac{1}{2})\bar{p}(-\frac{1}{2})$	-1
32.7964	0.8818	0.2526 $p(\frac{3}{2})\bar{p}(\frac{1}{2})$ -0.9044 $p(\frac{3}{2})p(\frac{1}{2})$	+2
32.7964	0.8818	0.2526 $p(-\frac{3}{2})\bar{p}(-\frac{1}{2})$ -0.9044 $p(-\frac{3}{2})p(-\frac{1}{2})$	-2
33.8494	0.8840	-0.4676 $\bar{p}(-\frac{1}{2})\bar{p}(\frac{1}{2})$ +0.5759 $p(-\frac{1}{2})p(\frac{1}{2})$ -0.5759 $p(-\frac{3}{2})p(\frac{3}{2})$	0
33.9900	0.8749	0.4677 $p(\frac{1}{2})\bar{p}(\frac{1}{2})$ -0.8100 $p(\frac{3}{2})\bar{p}(-\frac{1}{2})$	+1
33.9900	0.8749	0.8100 $p(-\frac{3}{2})\bar{p}(\frac{1}{2})$ -0.4677 $p(-\frac{1}{2})\bar{p}(-\frac{1}{2})$	-1
33.9900	0.8749	-0.6614 $p(-\frac{1}{2})\bar{p}(\frac{1}{2})$ +0.6614 $\bar{p}(-\frac{1}{2})p(\frac{1}{2})$	0
34.9468	0.8744	-0.4501 $p(-\frac{3}{2})\bar{p}(\frac{1}{2})$ +0.2532 $p(-\frac{3}{2})p(\frac{1}{2})$ -0.7796 $p(-\frac{1}{2})\bar{p}(-\frac{1}{2})$	-1
34.9468	0.8744	0.7796 $p(\frac{1}{2})\bar{p}(\frac{1}{2})$ +0.4501 $p(\frac{3}{2})\bar{p}(-\frac{1}{2})$ -0.2532 $p(\frac{3}{2})p(-\frac{1}{2})$	+1
34.9468	0.8744	-0.9001 $p(\frac{3}{2})\bar{p}(\frac{1}{2})$ -0.2532 $p(\frac{3}{2})p(\frac{1}{2})$	+2
34.9468	0.8744	-0.9001 $p(-\frac{3}{2})\bar{p}(-\frac{1}{2})$ -0.2532 $p(-\frac{3}{2})p(-\frac{1}{2})$	-2
34.9468	0.8744	0.6365 $p(-\frac{1}{2})\bar{p}(\frac{1}{2})$ +0.6365 $\bar{p}(-\frac{1}{2})p(\frac{1}{2})$ -0.1790 $p(-\frac{1}{2})p(\frac{1}{2})$ -0.1790 $p(-\frac{3}{2})p(\frac{3}{2})$	0
37.4880	0.8945	-0.8070 $\bar{p}(-\frac{1}{2})\bar{p}(\frac{1}{2})$ -0.3383 $p(-\frac{1}{2})p(\frac{1}{2})$ +0.3383 $p(-\frac{3}{2})p(\frac{3}{2})$	0

TABLE IV: Double ionization potentials (DIPs, in eV) and pole strengths (PS) for the $2h$ final states of *gerade* symmetry in jj coupling. The $p(\bar{p})$ symbols denote the $p_{\frac{3}{2}}$ ($p_{\frac{1}{2}}$) spinors and the corresponding individual m_j projections are given in parentheses. $M_J = m_{j_1} + m_{j_2}$.

Additionally, the proper inclusion of spin-orbit coupling becomes evident when a scalar relativistic propagator calculation is performed setting out from the spin-free Hamiltonian (table V). Now the double ionization potentials (DIPs) exhibit a ninefold, fivefold and one-fold degeneracy corresponding to the ^3P, ^1D and ^1S LS-coupled manifold of a $5p^4$ electron configuration and only two transitions at 9630.3 cm^{-1} and 27087.3 cm^{-1} can be predicted where just the first one is in reasonable agreement with experiment. Obviously, this spin-free description is inadequate even for a qualitatively correct interpretation of the spectrum.

The spin-free final state classifications in table V occur with respect to Cartesian p_x, p_y and p_z orbitals obtained in D_{2h} symmetry. The spin projections (M_S values) can be read off directly from the final state configurations in table V and for a proper M_L assignment

DIP	PS	Configurations	M_S
33.4693	0.8778	0.66249 $p_{z\beta}p_{y\alpha}$ -0.66249 $p_{y\beta}p_{z\alpha}$	0
33.4693	0.8778	0.66249 $p_{z\beta}p_{x\alpha}$ -0.66249 $p_{x\beta}p_{z\alpha}$	0
33.4693	0.8778	-0.66249 $p_{y\beta}p_{x\alpha}$ +0.66249 $p_{x\beta}p_{y\alpha}$	0
33.4693	0.8778	-0.93690 $p_{z\alpha}p_{y\alpha}$	1
33.4693	0.8778	0.93690 $p_{z\alpha}p_{x\alpha}$	1
33.4693	0.8778	0.93690 $p_{z\beta}p_{y\beta}$	-1
33.4693	0.8778	0.93690 $p_{z\beta}p_{x\beta}$	-1
33.4693	0.8778	-0.93690 $p_{y\alpha}p_{x\alpha}$	1
33.4693	0.8778	0.93690 $p_{y\beta}p_{x\beta}$	-1
34.6633	0.8767	0.19955 $p_{x\beta}p_{x\alpha}$ -0.73886 $p_{y\beta}p_{y\alpha}$ +0.53930 $p_{z\beta}p_{z\alpha}$	0
34.6633	0.8767	0.66203 $p_{z\beta}p_{y\alpha}$ +0.66203 $p_{y\beta}p_{z\alpha}$	0
34.6633	0.8767	0.66203 $p_{z\beta}p_{x\alpha}$ +0.66203 $p_{x\beta}p_{z\alpha}$	0
34.6633	0.8767	-0.66203 $p_{y\beta}p_{x\alpha}$ -0.66203 $p_{x\beta}p_{y\alpha}$	0
34.6633	0.8767	0.73795 $p_{x\beta}p_{x\alpha}$ -0.19616 $p_{y\beta}p_{y\alpha}$ -0.54179 $p_{z\beta}$ $p_{z\alpha}$	0
36.8277	0.9066	-0.54485 $p_{x\beta}p_{x\alpha}$ -0.54485 $p_{y\beta}p_{y\alpha}$ -0.54485 $p_{z\beta}p_{z\alpha}$	0

TABLE V: Spin-free (LS coupled) DIPs (in eV) and pole strengths (PS) for the final states of *gerade* symmetry derived from the $5p^4$ configuration of xenon. The most prominent change compared to the DC-ADC2 is the high degree of degeneracy and the concomitant loss of spectral structure. The configurations are to be understood as being totally antisymmetric with respect to particle interchange.

suitable linear combinations within the degenerate manifolds are to be formed. Similar to the four-component calculation the spin-free states resemble a Hartree-Fock state but with additional contributions accounting for electron correlation.

As it was mentioned in section I the propagator method gives immediate access to the complete final state manifold where the pole strengths relate to the peak heights in the spectrum. The coefficients of the participating $2h$ configurations constituting a specific final state can hereby be obtained from the eigenvector. Employing this information, a theoretical spectrum can be immediately generated. In order to compare the DC-ADC2 stick spectrum to the experimental one possessing a natural linewidth we convolve the theoretical spectrum with Lorentzian envelopes. Hereby the reported spectroscopic resolution serves as the full

width at half maximum (FWHM) value which was taken as $\Gamma = 50$ meV for the Xe and Br_2 spectrum. The simulated peaks which appear at the energies E_i then attain the following functional form:

$$L_i(E) = \frac{1}{\pi} \frac{\Gamma/2}{(E - E_i)^2 + (\Gamma/2)^2} \,. \tag{16}$$

The total spectrum $I_{tot}(E)$ is obtained by summing over all contributions $L_i(E)$ multiplied by the pole strength X_i obtained from the DC-ADC2 calculation as

$$I_{tot}(E) = \sum_i L_i(E) X_i \,. \tag{17}$$

The simulated experimental Xe^{2+} spectrum is shown in Fig. 2 and the lowest DIP was shifted to the experimental onset. The areas under the peaks exhibit conformity with the statistical weights of the populated levels and the theoretical spectrum well resembles the experimental one in [43].

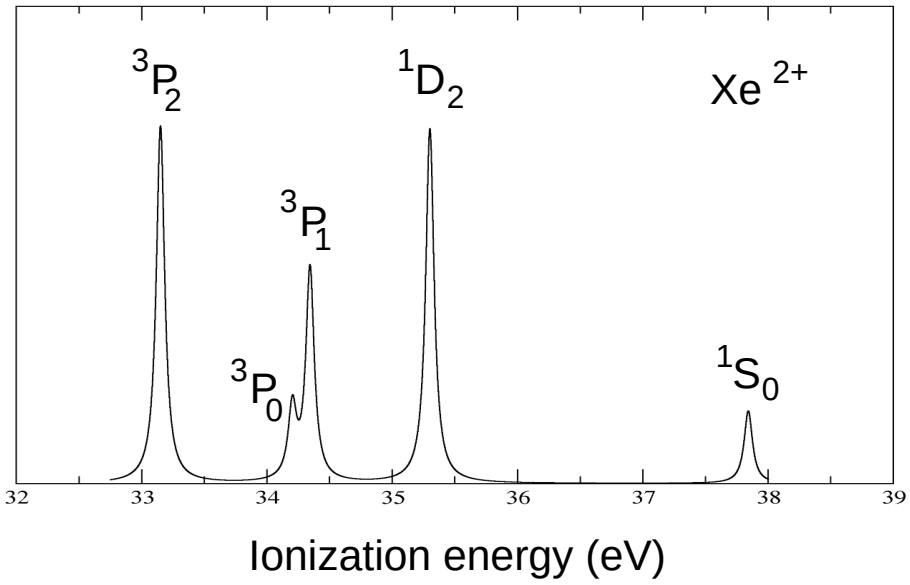

FIG. 2: Simulated experimental Xe^{2+} spectrum obtained from the stick spectrum by convolution with a Lorentzian curve and shifted to the experimental onset.

B. Molecular bromine

Recently, Fleig et al. calculated potential energy curves for the lowest g and u states of Br_2^{2+} and proposed a new double ionization mechanism [21]. For the determination of the dicationic final states relativistic CI [44, 45] and MRCC approaches [46, 47] together with a large ANO-RCC basis were employed. It is therefore of prominent interest to compare our propagator approach to these wave function-based results. It was not our intention to reproduce the Br_2^{2+} potential energy curves for a characterization of special ionization processes proposed in [21] but to demonstrate the usefulness of the four-component propagator approach with respect to final state and spectrum analysis for this molecule. The orbital energy diagram at the self consistent field level for the outer valence p orbitals is shown in Fig. 3 obtained with the Lévy-Leblond (nonrelativistic), the spin-free (purely scalar relativistic) and Dirac-Coulomb Hamiltonian (scalar relativistic and spin-orbit).

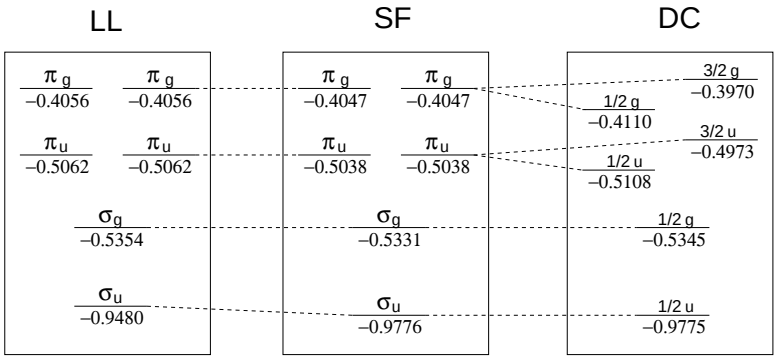

FIG. 3: Orbital energy diagram (in a.u.) for the outer valence p space of neutral Br_2 obtained with the Lévy-Leblond (LL), the spin-free (SF) and Dirac-Coulomb (DC) Hamiltonian.

One observes an average spin-orbit splitting of 6.9 mH for the π_g, π_u outer valence orbitals that prevails over scalar relativistic energy changes of 1.0 - 2.4 mH. Due to open $\pi_{g,u}$ shells in Br_2^{2+} spin-orbit coupling will play a role in the corresponding spectra. The classification of the molecular orbitals follows the $\Lambda\Sigma$ and Ω coupling schemes, respectively. For the onset of the double ionization Fleig et al. obtained a value of 26.94 eV compared to the experimental onset of 28.55 eV (vertical) and 28.25 eV (adiabatic) [15] where in the ADC2 approach 27.39 eV (DC-ADC2) and 27.54 eV (SF-ADC2) were obtained. The interplay of electron correlation and relaxation effects together with spin-orbit coupling is rather involved and puts high demands on the theoretical methodology. The deviations of the DC-ADC2

DIPs from experiment mainly result from an insufficient inclusion of electron relaxation effects which are larger for a double ionized final state than for excited or singly ionized final states. This deficiency could be cured by increasing the order of the perturbation treatment but will not distort the physical picture obtained from the current calculations. It should be mentioned that a *strict* second order DC-ADC where the $3h1p/3h1p$ particle (satellite) block is included only in zeroth order would be too inaccurate and the additional first order contributions (the various $V_{ab,[cd]}$ terms in eq. (9)) considerably improve on the final state energies. It is common practice to use this so-called *extended* ADC2 routinely as can be seen from eq. (9) where these first order contributions are included. The satellite block will not change any further when it comes to an extension to third-order.

The energy differences of the outer valence final state energies obtained at the DC-ADC2 and wave function-based level of Fleig et al. exhibit an average deviation of 0.084 eV (see table VI). With the exception of the DIP onset a good agreement between both approaches is therefore observed.

The second aspect to be addressed is the comparison of the individual final state compositions. Table VII lists the DC-ADC2 DIPs and pole strengths together with the detailed configuration information for the 10 lowest final states in Br_2^{2+}. Hereby the explicit Kramers partners occurring in the degenerate $\pm\Omega$ pairs are reported separately. All outer valence states can be identified as main states which are states of high pole strength and no significant admixture of $3h1p$ configurations. This is beneficial for a future two-hole population analysis because for main states it suffices to include the $2h$ space in the population analysis without loss of accuracy [48].

Ω	$\Delta^{a)}$	$\Delta^{b)}$	Ω	$\Delta^{a)}$	$\Delta^{b)}$
0_g	0.000	0.000	3_u	1.538	1.418
1_g	0.126	0.149	2_u	1.882	1.774
2_g	0.639	0.622	1_u	1.949	1.854
0_g	1.134	1.059	0_u	2.207	2.112
0_u	1.491	1.365	1_u	2.229	2.133

TABLE VI: Energy differences Δ (in eV) of the individual Ω-coupled states to the lowest state of Br_2^{2+}. States with $\Omega \neq 0$ are doubly degenerate. a) Our work, b) Ref. [21].

For a direct comparison of a specific final state configuration one has to account for the different notations employed in [21] and in our work (table VII). We report the spinors where the hole was created (indicated by the -1 superscript) whereas Fleig et al. list the remaining *occupied* spinors after the double ionization. In this respect we find a dominant $\bar{\pi}^{-1}_{3/2g}\pi^{-1}_{3/2g}$, a less pronounced $\bar{\pi}^{-1}_{1/2g}\pi^{-1}_{1/2g}$ and a weak $\bar{\pi}^{-1}_{3/2u}\pi^{-1}_{3/2u}$ contribution to the Br_2^{2+} ground state which also seems natural from an energetic point of view (see Fig. 3). Fleig et al. report for this state a $0.84\pi^2_{g1/2} - 0.37\pi^2_{g3/2} - 0.23\pi^2_{u1/2}\pi^2_{g1/2}\pi^2_{g3/2}$ configuration well matching with our result apart from a different phase in the $\bar{\pi}^{-1}_{1/2g}\pi^{-1}_{1/2g}(\pi^2_{g3/2})$ part. A detailed analysis of the other states reveals some additional contributions to the second 0_g state in DC-ADC2, namely the $\bar{\pi}^{-1}_{1/2u}\pi^{-1}_{1/2u}$ and $\bar{\pi}^{-1}_{3/2u}\pi^{-1}_{3/2u}$ determinants (table VII) in contrast to an expansion in pure *gerade* $(0.81 + 0.33)\pi^2_{3/2g}\pi^2_{1/2g}$ orbitals reported in [21]. The remaining states in this energy range exhibit a good resemblance to the wave function-based results. Already for the ground state of the doubly ionized system considerable configuration mixing is observed which can not be reproduced by a single reference self consistent field calculation. This strong configuration mixing is quite characteristic for doubly ionized states and is already observed in light systems such as BF_3 [48]. This is in contrast to outer valence final states of singly ionized systems which in most cases possess only one major contribution in the intermediate state representation [29]. Due to the relevance of spin-orbit coupling for a correct interpretation of the spectral structure spin-free results are not discussed here.

In an analogous way we convoluted the Br_2^{2+} stick spectrum with Lorentzian curves in the energy range of 28 and 32 eV (Fig. 4) in order to simulate the experimental spectrum. The experimental peak positions in table VIII together with their nonrelativistic designations were obtained by Yencha et al. [15]. Hereby the $a^1\Delta_g$ and the $^3\Delta_u$ states will undergo spin-orbit splitting.

Comparing the theoretical spectrum with the experimental threshold photoelectron coincidence spectrum one finds a substantial discrepancy of the intensities for the lowest u states (indicated by the dashed box in Fig. 4). The intensity of a transition is controlled by the magnitude of the transition matrix element including the initial and final state wave function. In the absence of strong vibronic coupling effects one can in a first approximation write the full wave function as a product of an electronic and nuclear part yielding additional overlap matrix elements over nuclear wave functions, the well-known Franck-Condon (FC) factors. By extensive calculations Fleig et al. found a purely repulsive character of

DIP (eV)	PS	Final state configuration	Ω
27.393	0.8574	$0.40229\bar{\pi}^{-1}_{1/2g}\pi^{-1}_{1/2g}$ $+0.81293\bar{\pi}^{-1}_{3/2g}\pi^{-1}_{3/2g}$ $-0.18101\bar{\pi}^{-1}_{3/2u}\pi^{-1}_{3/2u}$	0g
27.519	0.8539	$-0.90975\pi^{-1}_{3/2g}\bar{\pi}^{-1}_{1/2g}$ $-0.15729\pi^{-1}_{3/2u}\bar{\pi}^{-1}_{1/2u}$	+1g
27.519	0.8539	$0.90975\bar{\pi}^{-1}_{3/2g}\pi^{-1}_{1/2g}$ $+0.15729\bar{\pi}^{-1}_{3/2u}\pi^{-1}_{1/2u}$	-1g
28.032	0.8668	$-0.88962\pi^{-1}_{3/2g}\pi^{-1}_{1/2g}$ $+0.27335\pi^{-1}_{3/2u}\pi^{-1}_{1/2u}$	+2g
28.032	0.8668	$-0.88962\bar{\pi}^{-1}_{3/2g}\bar{\pi}^{-1}_{1/2g}$ $+0.27335\bar{\pi}^{-1}_{3/2u}\bar{\pi}^{-1}_{1/2u}$	-2g
28.527	0.8712	$-0.78746\bar{\pi}^{-1}_{1/2g}\pi^{-1}_{1/2g}$ $+0.36346\bar{\pi}^{-1}_{3/2g}\pi^{-1}_{3/2g}$ $+0.26375\bar{\pi}^{-1}_{1/2u}\pi^{-1}_{1/2u}$ $-0.21103\bar{\pi}^{-1}_{3/2u}\pi^{-1}_{3/2u}$	0g
28.884	0.8777	$0.65611\bar{\pi}^{-1}_{3/2u}\pi^{-1}_{3/2g}$ $-0.65611\pi^{-1}_{3/2u}\bar{\pi}^{-1}_{3/2g}$	0u
28.931	0.8806	$0.93841\pi^{-1}_{3/2u}\pi^{-1}_{3/2g}$	+3u
28.931	0.8806	$-0.93841\bar{\pi}^{-1}_{3/2u}\bar{\pi}^{-1}_{3/2g}$	-3u
29.275	0.8782	$-0.65854\pi^{-1}_{3/2u}\pi^{-1}_{1/2g}$ $+0.66591\pi^{-1}_{1/2u}\pi^{-1}_{3/2g}$	+2u
29.275	0.8782	$-0.65854\bar{\pi}^{-1}_{3/2u}\bar{\pi}^{-1}_{1/2g}$ $+0.66591\bar{\pi}^{-1}_{1/2u}\bar{\pi}^{-1}_{3/2g}$	-2u
29.342	0.8783	$-0.65105\pi^{-1}_{3/2u}\bar{\pi}^{-1}_{1/2g}$ $-0.67280\bar{\pi}^{-1}_{1/2u}\pi^{-1}_{3/2g}$	+1u
29.342	0.8783	$0.65105\bar{\pi}^{-1}_{3/2u}\pi^{-1}_{1/2g}$ $+0.67280\pi^{-1}_{1/2u}\bar{\pi}^{-1}_{3/2g}$	-1u
29.600	0.8742	$0.65371\bar{\pi}^{-1}_{1/2u}\pi^{-1}_{1/2g}$ $-0.65371\pi^{-1}_{1/2u}\bar{\pi}^{-1}_{1/2g}$	0u
29.622	0.8757	$0.93404\pi^{-1}_{1/2u}\pi^{-1}_{1/2g}$	+1u
29.622	0.8757	$-0.93404\bar{\pi}^{-1}_{1/2u}\bar{\pi}^{-1}_{1/2g}$	-1u

TABLE VII: DC-ADC2 DIPs (in eV) and pole strengths (PS) for the 10 lowest $2h$ final states of Br_2^{2+}. States with $\Omega \neq 0$ are doubly degenerate and the configurations are totally antisymmetric with respect to particle interchange. A Kramers partner is indicated by a barred symbol and π denotes the fourfold degenerate parent orbital before inclusion of spin-orbit coupling.

the lowest excited u states of Br_2^{2+} in contrast to the bound $0_g(1), 1_g(1), 2_g(1)$ and $0_g(2)$ states supporting vibrational levels. It has been shown that in case of an excitation to a decaying state complicated nuclear dynamics lead to a substantially altered spectral structure [49]. This obviously happens in the considered spectral range for the u states of Br_2^{2+}. Additionally, energies and band shapes are strongly influenced by vibrational motion and Franck-Condon factors therefore should be taken into account if one seeks a reliable prediction of these spectra [50, 51]. The purely electronic DC-ADC2 results do not incorporate

State	Energy /eV
$X^3\Sigma_g^-$	28.55
$a^1\Delta_g$	29.03
$b^1\Sigma_g^+$	29.54
$^1\Sigma_u^-$	30.54
$^3\Sigma_u^+$	31.22
$^3\Delta_u$	31.75

TABLE VIII: Vertical double-ionization potentials in the low-energy region of Br_2^{2+} taken from [15].

these nuclear effects and lead to deviations for the decaying u states. For the bound states of Br_2^{2+}, however, a good agreement with experiment is observed already without the inclusion of nuclear effects.

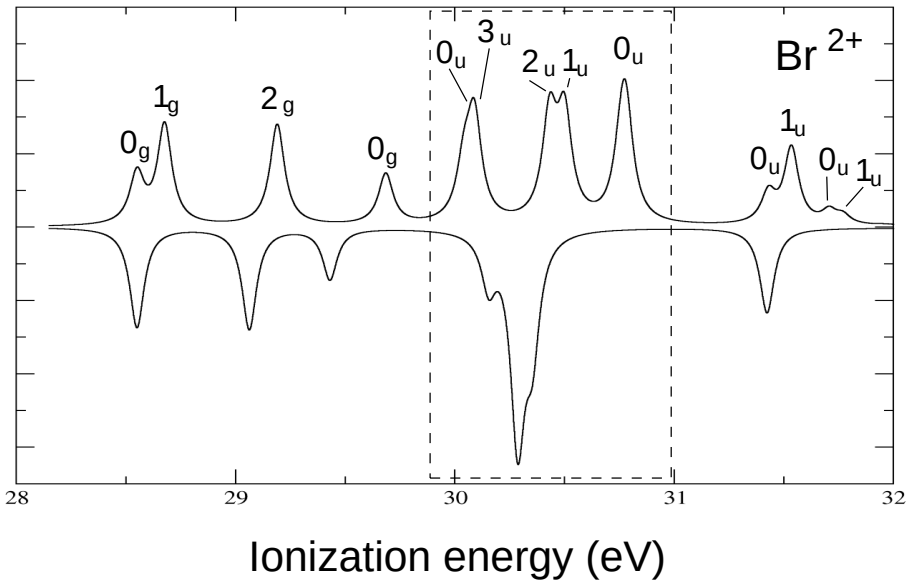

FIG. 4: Theoretical four-component (upward peaks) and scalar relativistic (downward peaks) double ionization spectrum of molecular bromine without FC factors and shifted to the experimental onset at 28.55 eV. In the experiment the *ungerade* features (dashed box) are only weakly visible due to their repulsive character. An assignment of the spin-free peaks is not done.

A substantial alteration of the spectrum takes place if spin-orbit contributions are omit-

ted as can be seen from the lower part of Fig. 4. The main changes hereby comprise a reduced structure, partial peak shifts and alterated intensities especially for the u states. The DIP onset for the spin-free spectrum is by 0.2 eV higher than the DC-ADC2 onset and the theoretical spectrum was also shifted to the experimental DIP onset. Obviously the spectral features even for the moderately relativistic bromine molecule are not reproducible by ignoring spin-orbit coupling in the propagator calculations, a situation which will become more pronounced in heavier systems.

V. SUMMARY

In this work we have shown the methodology and capability of the four-component two-particle propagator for spectrum analysis and final state classification. The efficient exploitation of symmetry in the integral handling and ADC matrix construction was demonstrated and the performance tested on two systems, the xenon atom and the bromine molecule. These calculations showed that without a proper account for relativistic effects neither of the two spectra can be adequately described. Compared to the high-level four-component multi-reference coupled cluster treatments our results are in excellent agreement with respect to line spacings and state analysis, already at the extended second-order stage of the propagator implementation. The deviations from experiment especially in the intensities for the u states can be understood by not accounting for nuclear dynamical effects occurring after excitation into decaying states. Subsequent analysis will be extended by inclusion of vibrational effects and a two-hole population analysis allowing for a detailed insight into electronic decay processes of clusters containing heavy elements. Already in the case of the moderately relativistic bromine molecule inclusion of spin-orbit coupling is mandatory for a reasonable resemblance of the experimental structure. Due to its second-order character the DC-ADC matrix construction scales similarly to the second-order Møller-Plesset (MP2) method and at the moment the AO→MO integral transformation and the band Lanczos diagonalization represent the computational bottlenecks in large DC-ADC2 calculations.

VI. ACKNOWLEDGMENTS

The author gratefully acknowledges financial support by the Deutsche Forschungsgemeinschaft.

---

[1] W. J. Griffiths, S. Svensson, A. Naves de Brito, N. Correia, C. J. Reid, M. L. Langford, F. M. Harris, C. M. Liegener, and H. Ågren, Chem. Phys. **173**, 109 (1993).

[2] W. J. Griffiths and M. Harris, Int. J. Mass Spectrom. Ion Process. **85**, 69 (1988).

[3] F. M. Harris and B. C. Cooper, Int. J. Mass Spectrom. Ion Process. **97**, 165 (1990).

[4] T. Masuoka and A. Kobayashi, J. Chem. Phys. **113**, 1559 (2000).

[5] D. M. Curtis and J. H. D. Eland, Int. J. Mass Spectrom. Ion Process. **63**, 241 (1985).

[6] J. H. D. Eland, L. A. Coles, and H. Bountra, Int. J. Mass Spectrom. Ion Process. **89**, 265 (1989).

[7] K. Codling, L. J. Frasinski, P. A. Hatherly, M. Stankiewicz, and F. P. Larkins, J. Phys. B: At. Mol. Opt. Phys. **24**, 951 (1991).

[8] R. I. Hall, L. Avaldi, G. Dawber, A. G. McConkey, M. A. MacDonald, and G. C. King, Chem. Phys. **187**, 125 (1994).

[9] F. O. Gottfried, L. S. Cederbaum, and F. Tarantelli, J. Chem. Phys. **104**, 9754 (1996).

[10] M. Hochlaf and J. H. D. Eland, J. Chem. Phys. **123**, 164314 (2005).

[11] R. Feifel, J. H. D. Eland, L. Storchi, and F. Tarantelli, J. Chem. Phys. **122**, 144309 (2005).

[12] S. Taylor, J. H. D. Eland, and M. Hochlaf, J. Chem. Phys. **124**, 204319 (2006).

[13] R. Feifel, J. H. D. Eland, and D. Edvardsson, J. Chem. Phys. **122**, 144308 (2005).

[14] J. T. Herron and V. H. Dibeler, J. Chem. Phys. **32**, 1884 (1960).

[15] A. J. Yencha, S. P. Lee, and G. C. King, in: Proceedings of the XXIV ICPEAC Conference (2005).

[16] D. Edvardsson, A. Danielsson, L. Karlsson, and J. H. D. Eland, Chem. Phys. **324**, 674 (2006).

[17] D. Edvardsson, A. Danielsson, L. Karlsson, and J. H. D. Eland, Chem. Phys. **332**, 249 (2007).

[18] A. Pilcher-Clayton and J. H. D. Eland, J. Electr. Spectrosc. Relat. Phenom. **142**, 313 (2005).

[19] L. S. Cederbaum, J. Zobeley, and F. Tarantelli, Phys. Rev. Lett. **79**, 4778 (1997).

[20] J. Zobeley, R. Santra, and L. S. Cederbaum, J. Chem. Phys. **115**, 5076 (2001).

[21] T. Fleig, D. Edvardsson, S. T. Banks, and J. H. D. Eland, Chem. Phys. **343**, 270 (2008).

[22] M. Pernpointner and A. B. Trofimov, J. Chem. Phys. **120**, 4098 (2004).

[23] G. Pestka, M. Bylicki, and J. Karwowski, J. Phys. B: At. Mol. Opt. Phys. **39**, 2979 (2006).

[24] H. Lehmann, Nuovo Cimento **11**, 342 (1954).

[25] J. Schirmer and A. Barth, Z. Phys. A **317**, 267 (1984).

[26] F. Tarantelli and L. S. Cederbaum, Phys. Rev. A **39**, 1639 (1989).

[27] F. Tarantelli and L. S. Cederbaum, Phys. Rev. A **39**, 1656 (1989).

[28] F. Tarantelli, Chem. Phys. **329**, 11 (2006).

[29] J. Schirmer, Phys. Rev. A **43**, 4647 (1991).

[30] J. Schirmer, L. S. Cederbaum, and O. Walter, Phys. Rev. A **28**, 1237 (1983).

[31] L. S. Cederbaum, W. Domcke, J. Schirmer, and W. von Niessen, Adv. Chem. Phys. **65**, 115 (1986).

[32] DIRAC, a relativistic ab initio electronic structure program, Release DIRAC08 (2008), written by L. Visscher, H. J. Aa. Jensen, and T. Saue, with new contributions from R. Bast, S. Dubillard, K. G. Dyall, U. Ekström, E. Eliav, T. Fleig, A. S. P. Gomes, T. U. Helgaker, J. Henriksson, M. Iliaš, Ch. R. Jacob, S. Knecht, P. Norman, J. Olsen, M. Pernpointner, K. Ruud, P. Sałek, and J. Sikkema (see http://dirac.chem.sdu.dk).

[33] L. Visscher, T. J. Lee, and K. G. Dyall, J. Chem. Phys. **105**, 8769 (1995).

[34] W. Kutzelnigg, Int. J. Quantum Chem. **25**, 107 (1984).

[35] K. G. Dyall, J. Chem. Phys. **100**, 2118 (1994).

[36] S. Urbaczek (Diploma thesis, Heidelberg, 2008).

[37] K. G. Dyall, Theor. Chem. Acc. **115**, 441 (2006).

[38] K. Huber and G. Herzberg, *Molecular Spectra and Molecular Structure Constants of Diatomic Molecules* (Van Nostrand, New York, 1979).

[39] W. Persson, C.-G. Wahlström, G. Bertuccelli, H. O. Di Rocco, J. G. Reyna Almandos, and M. Gallardo, Phys. Scripta **38**, 347 (1988).

[40] T. X. Carroll, J. D. Bozek, E. Kukk, V. Myrseth, L. J. Sæthre, T. D. Thomas, and K. Wiesner, J. Electr. Spectrosc. Relat. Phenom. **125**, 127 (2002).

[41] K. D. Dyall, I. P. Grant, F. A. Parpia, and E. P. Plummer, Comput. Phys. Commun. **55**, 425 (1989).

[42] K. G. Dyall and K. Fægri, Theor. Chim. Acta **94**, 39 (1996).

[43] J. H. D. Eland, Adv. Chem. Phys. **141**, 103 (2009).

[44] T. Fleig, J. Olsen, and L. Visscher, J. Chem. Phys. **119**, 2963 (2003).

[45] T. Fleig, H. Jensen, J. Olsen, and L. Visscher, J. Chem. Phys. **124**, 104106 (2006).

[46] J. Olsen, J. Chem. Phys. **113**, 7140 (2000).

[47] J. W. Krogh and J. Olsen, Chem. Phys. Lett. **344**, 578 (2001).

[48] F. Tarantelli, A. Sgamellotti, and L. S. Cederbaum, J. Chem. Phys. **94**, 523 (1991).

[49] L. S. Cederbaum and F. Tarantelli, J. Chem. Phys. **98**, 9691 (1993).

[50] F. Tarantelli, L. S. Cederbaum, and A. Sgamellotti, J. Electr. Spectrosc. Relat. Phenom. **76**, 47 (1995).

[51] K. Zähringer, H. Meyer, L. S. Cederbaum, F. Tarantelli, and A. Sgamellotti, Chem. Phys. Lett. **206**, 247 (1993).